Pharmaceutical Analytical Chemistry: Open Access

Trivedi et al., Pharm Anal Chem Open Access 2015, 1:1
DOI: 10.4172/2471-2698.1000102

Research Article Open Access

Physicochemical and Spectroscopic Characterization of Biofield Energy Treated *p*-Anisidine

Mahendra Kumar Trivedi[1], Alice Branton[1], Dahryn Trivedi[1], Gopal Nayak[1], Khemraj Bairwa[2] and Snehasis Jana[2*]

[1]*Trivedi Global Inc., 10624 S Eastern Avenue Suite A-969, Henderson, NV 89052, USA*
[2]*Trivedi Science Research Laboratory Pvt. Ltd., Hall-A, Chinar Mega Mall, Chinar Fortune City, Hoshangabad Rd., Bhopal, Madhya Pradesh, India*

Abstract

The *p*-anisidine is widely used as chemical intermediate in the production of various dyes, pigments, and pharmaceuticals. This study was aimed to evaluate the effect of biofield energy treatment on the physicochemical and spectroscopic properties of *p*-anisidine. The study was performed after dividing the sample in two groups; one was remained as untreated and another was subjected to Mr. Trivedi's biofield energy treatment. Afterward, both the control and treated samples of *p*-anisidine were evaluated using X-ray diffraction (XRD), surface area analyzer, differential scanning calorimetry (DSC), thermogravimetric analysis-derivative thermogravimetry (TGA-DTG), Fourier transform infrared (FT-IR), and ultraviolet-visible (UV-Vis) spectroscopy. The XRD analysis showed the increase in unit cell volume from 683.81 → 690.18 × 10^{-24} cm^3 and crystallite size from 83.84→84.62 nm in the treated sample with respect to the control. The surface area analysis exhibited the significant increase (25.44%) in the surface area of treated sample as compared to control. The DSC thermogram of control *p*-anisidine showed the latent heat of fusion and melting temperature and 146.78 J/g and 59.41°C, respectively, which were slightly increased to 148.89 J/g and 59.49°C, respectively after biofield treatment. The TGA analysis showed the onset temperature of thermal degradation at 134.68°C in the control sample that was increased to 150.02°C after biofield treatment. The result showed about 11.39% increase in onset temperature of thermal degradation of treated *p*-anisidine as compared to the control. Moreover, the T_{max} (temperature at which maximum thermal degradation occurs) was also increased slightly from 165.99°C (control) to 168.10°C (treated). This indicated the high thermal stability of treated *p*-anisidine as compared to the control. However, the FT-IR and UV spectroscopic studies did not show any significant changes in the spectral properties of treated *p*-anisidine with respect to the control.

All together, the XRD, surface area and thermal analysis suggest that Mr. Trivedi's biofield energy treatment has the impact on physical and thermal properties of the treated *p*-anisidine.

Keywords: *p*-Anisidine; X-ray diffraction; Surface area analysis; Differential scanning calorimetry; Fourier transform infrared; Biofield energy

Abbreviations

NIH: National Institute of Health; NCCAM: National Center for Complementary and Alternative Medicine; XRD: X-ray diffraction; DSC: Differential scanning calorimetry; TGA: Thermogravimetric analysis; DTG: Derivative Thermogravimetry; FT-IR: Fourier transforms infrared

Introduction

Anisidine is an aromatic amine (methoxyaniline) and exists in three isomeric forms *i.e., ortho, meta,* and *p*-anisidine [1]. The *p*-anisidine is widely used as an intermediate in the production of numerous azo and triphenylmethane dyes, and pigments. It is also used in the production of pharmaceuticals including the guaiacol expectorant [2], as an antioxidant for polymercaptan resins, and as a corrosion inhibitor for steel [3]. Apart from the beneficial use of *p*-anisidine, it is toxic for human beings. The acute exposure may cause skin irritation, whereas the chronic exposure may cause headaches, vertigo, and blood complications like sulfhemoglobin, and methemoglobin [3,4]. The oral exposure to anisidine hydrochloride resulted in cancer of the urinary bladder in male and female rats [5]. By considering the importance of *p*-anisidine as an intermediate for the production of various dyes, pharmaceuticals and several other organic products, it is advantageous to find out an alternate approach that can enhance the physicochemical and thermal properties of *p*-anisidine in the useful way.

Recently, healing therapy or therapeutic touch is used as an alternative treatment approach in several fields, and known as the biofield energy treatment. The National Institute of Health/National Center for Complementary and Alternative Medicine (NIH/NCCAM) considered the biofield energy (putative energy fields) treatment in the subcategory of energy therapies used to promote health and healing [6,7]. The biofield treatment is being applied in the healing process to reduce the anxiety, pain, and to promote the overall health of human being [8,9]. Previously, it was reported that all the electrical processes occurring in the human body have strong correlation with the magnetic field [10]. It is well known that moving charged particles like ions, atoms, electrons etc. produces the electromagnetic radiation [11]. Similarly, the moving ions, and charged particles in the human body also produced the bioenergetic field that permeates and surrounding the human body. This bioenergetic field is called as biofield and energy associated with this field is known as the biofield energy [12]. The effect of biofield has been reported by several researchers on bacterial cultures [13], antibiotics, proteins [14], and conformational change in

***Corresponding author:** Snehasis Jana, Trivedi Science Research Laboratory Pvt. Ltd., Hall-A, Chinar Mega Mall, Chinar Fortune City, Hoshangabad Rd., Bhopal-462 026, Madhya Pradesh, India, Tel: +91-755-6660006; E-mail: publication@trivedisrl.com

Received September 09, 2015; **Accepted** September 19, 2015; **Published** September 27, 2015

Citation: Trivedi MK, Branton A, Trivedi D, Nayak G, Bairwa K, et al (2015) Physicochemical and Spectroscopic Characterization of Biofield Energy Treated *p*-Anisidine. Pharm Anal Chem Open Access 1: 102. doi:10.4172/2471-2698.1000102

DNA [15]. Thus, the human has the ability to harness the energy from the environment or Universe and transmit it to any living or nonliving object on the Globe. The object(s) receive the energy and respond into the useful way; this process is termed as biofield treatment. Mr. Trivedi's unique biofield energy treatment is also known as The Trivedi Effect®.

Recently, Mr. Trivedi's biofield energy treatment has been reported to alter the physicochemical and thermal properties of several metals and ceramics [16-18]. It has also been reported to alter the spectroscopic properties of various pharmaceutical drugs like chloramphenicol, tetracycline, metronidazole, and tinidazole [19,20]. Moreover, the biofield treatment has been studied in several fields like biotechnology research [21], agriculture research [22,23], and microbiology research [24,25].

Based on the significant impact of biofield energy treatment and chemical importance of *p*-anisidine, this study was aimed to evaluate the effect of Mr. Trivedi's biofield energy treatment on physicochemical and spectroscopic properties of *p*-anisidine using several analytical techniques like XRD, surface area analysis, DSC, TGA-DTG analysis, FT-IR and UV-vis spectroscopy.

Materials and Methods

Study design

The *p*-anisidine was purchased from Loba Chemie Pvt. Ltd., India. The *p*-anisidine was divided into two groups; one was remained untreated (control group) and another was coded as treated group. The treated group in sealed pack was handed over to Mr. Trivedi for biofield energy treatment under laboratory conditions. Mr. Trivedi provided the biofield energy treatment to the treated group through his unique energy transmission process without touching the sample. Afterward, both the control and treated samples of *p*-anisidine were analyzed using various analytical techniques like X-ray diffraction (XRD), surface area analysis, differential scanning calorimetry (DSC), thermogravimetric analysis (TGA), Fourier transform infrared (FT-IR), and ultraviolet-visible (UV-Vis) spectroscopy.

XRD study

The XRD analysis of the control and treated *p*-anisidine was carried out on Phillips, Holland PW 1710 X-ray diffractometer with nickel filter and copper anode. The wavelength used in XRD system was 1.54056 Å.

Percent change in unit cell volume was calculated using following equation

Percent change in unit cell volume=$[(V_t-V_c)/V_c] \times 100$

Here V_c and V_t are the unit cell volume of control and treated sample, respectively.

The molecular weight of atom was calculated using following equation:

Molecular weight=number of protons × weight of a proton+number of neutrons × weight of a neutron+number of electrons × weight of an electron.

Molecular weight in g/Mol was calculated from the weights of all atoms in a molecule multiplied by the Avogadro number (6.023×10^{23}). The percent change in molecular weight was calculated using the following equation:

Percent change in molecular weight=$[(M_t-M_c)/M_c] \times 100$

Here, M_c and M_t are molecular weight of control and treated sample, respectively.

Percentage change in crystallite size was calculated using following formula:

Percentage change in crystallite size=$[(G_t-G_c)/G_c] \times 100$

Here, G_c and G_t are crystallite size of control and treated powder samples, respectively.

Surface area analysis

The surface area of both the control and treated samples was evaluated using the Brunauer–Emmett–Teller (BET) surface area analyzer, Smart SORB 90. Percent change in surface area was computed using following equation:

$$\% \text{ change in surface area} = \frac{[S_{Treated} - S_{Control}]}{S_{Control}} \times 100$$

Here, $S_{Control}$ is the surface area of control sample and $S_{Treated}$ is the surface area of treated sample.

DSC study

The control and treated samples of *p*-anisidine were analyzed using a Pyris-6 Perkin Elmer differential scanning calorimeter. The heating rate was set to 10°C/min under air atmosphere with air flow rate of 5 mL/min. An empty pan sealed with cover was used as the reference pan. The melting temperature (T_m) and latent heat of fusion (ΔH) were obtained from the DSC thermogram.

TGA-DTG analysis

The TGA-DTG analysis was carried out in order to investigate the thermal stability of the control and treated *p*-anisidine. The studies were performed on Mettler Toledo simultaneous TGA-DTG system. Both the control and treated samples were heated from room temperature to 400°C with a heating rate of 5°C/min under air atmosphere. The onset temperature (at which thermal degradation started) and T_{max} (temperature at which maximum weight loss occur) in samples were obtained from DTG thermogram.

Spectroscopic studies

For the FT-IR and UV-Vis spectroscopic characterization, the treated sample was divided into two groups *i.e.,* T1 and T2. These treated groups were then analyzed using FT-IR and UV-Vis spectroscopy and data were compared with respective data of control sample.

FT-IR spectroscopic characterization

The samples for FT-IR spectroscopy were prepared by crushing with spectroscopic grade KBr into fine powder. Finally, the mixture was pressed into pellets with a hydraulic press and then used for FT-IR analysis. The spectrum was recorded on Shimadzu's Fourier transform infrared spectrometer (Japan) with the frequency range of 500-4000 cm^{-1}. The analysis was done to investigate the impact of biofield energy treatment at the atomic level like dipole moment, force constant, and bond strength in chemical structure [26].

UV-Vis spectroscopic analysis

The samples were prepared in methanol for UV spectroscopy. The UV spectra of the control and treated samples of *p*-anisidine were acquired on Shimadzu UV-2400 PC series spectrophotometer with quartz cuvette having slit widths of 2.0 nm. The wavelength of UV analysis was set in the range of 200-400 nm. This study was performed

to evaluate the impact of biofield energy treatment on the energy gap of highest occupied molecular orbital and lowest unoccupied molecular orbital (HOMO–LUMO) [27].

Results and Discussion

XRD analysis

The XRD diffractograms of control and treated *p*-anisidine are shown in Figure 1. The control sample exhibited the XRD peaks at 2θ equal to 12.98°, 13.19°, 18.68°, 18.89°, 22.20°, 25.70°, 26.10°, 26.63°, 28.01°, and 28.49°. Similarly, the XRD diffractogram of treated *p*-anisidine showed the XRD peaks at 2θ equal to 13.16°, 13.26°, 18.75°, 18.90°, 19.65°, 22.09°, 22.40°, 24.24°, 24.54°, and 28.31°. XRD diffractogram of both the control and treated *p*-anisidine showed the intense peaks that suggest the crystalline nature of *p*-anisidine. Figure 1 clearly showed the significant alteration in the intensity of XRD peaks in treated sample as compared to the control. In addition, control showed the most intense peak at 18.68, whereas it was found at 24.24 in treated sample. It was reported that the change in crystal morphology causes the alteration in relative intensities of the peaks [28]. Furthermore, the alteration in 2θ values of treated sample as compared to the control indicated that an internal strain was probably present in the treated sample [29]. It is assumed that the energy, which probably transferred through biofield treatment, might induce the internal strain in the treated sample.

The unit cell volume, molecular weight and crystallite size of control and treated *p*-anisidine were computed using Powder X software and data are depicted in Table 1. The unit cell volume of control and treated samples were found as 683.81 and 690.18 × 10^{-24} cm^3, respectively. The result showed slight increase in the unit cell volume in biofield treated sample as compared to control. Similarly, the molecular weight of treated sample was also increased slightly (0.93%) with respect to the control. It is hypothesized that the biofield energy possibly acted on treated *p*-anisidine crystals at nuclear level and altered the number of proton and neutrons as compared to the control, which may led to increase the molecular weight.

The crystallite size of the control *p*-anisidine was observed as 83.84 nm that was increased to 84.62 nm in the treated sample. The result suggests a small increase in crystallite size of treated sample as compared to the control. It was reported that increase in annealing temperature significantly affects the crystallite size of the materials. The increase in temperature leads to decrease in dislocation density and increase in number of unit cell, which ultimately causes an increase in crystallite size [30,31]. It is postulated that biofield treatment may provide some thermal energy to *p*-anisidine molecules. As a result, the dislocation density might be reduced and thus the number of unit cell and crystallite size was increased.

Surface area analysis

The surface area of control and treated samples of *p*-anisidine was determined using BET surface area analyzer and data are presented in Figure 2. The surface area of the control and treated sample was found as 0.4638 m^2/g and 0.5818 m^2/g, respectively. It showed a significant increase in surface area by 25.44% in the treated sample as compared to the control. It is well-reported that surface area is inversely proportional to the particle size [32]. Based on this, it was assumed that biofield energy treatment may provid the energy to the *p*-anisidine molecule that lead to reduction in particle size through energy milling [33]. In addition, the XRD data also indiacted that surface morpholgy of treated sample might changed after the biofield treatment, thus it could be a probable cause for increase in surface area. As a result the increase in surface area was observed in treated sample as compared to the control.

DSC analysis

DSC was used to determine the melting temperature and latent heat of fusion (ΔH) of the control and treated *p*-anisidine. DSC thermogram (Figure 3) of *p*-anisidine showed the melting temperature at 59.41°C in the control and 59.49°C in the treated sample (Table 2). The result suggests no change in melting temperature of treated sample as compared to the control. The melting temperature of control *p*-anisidine was well supported by literature data [34]. DSC thermogram exhibited the ΔH of 146.78 J/g in control sample and 148.89 J/g in the treated sample of *p*-anisidine. The result showed about 1.44% increase in latent heat of fusion after biofield energy treatment with respect to the control. The existence of internal strain was evidenced by XRD data. Thus, it is assumed that presence of strain might cause to move the molecules toward each other. As a result, the intermolecular interaction in the treated sample might increase after the biofield treatment and that might be responsible for increase in the latent heat of fusion. Recently, our group has reported the biofield energy induced alteration in the value of latent heat of fusion of some metals like lead and tin [17].

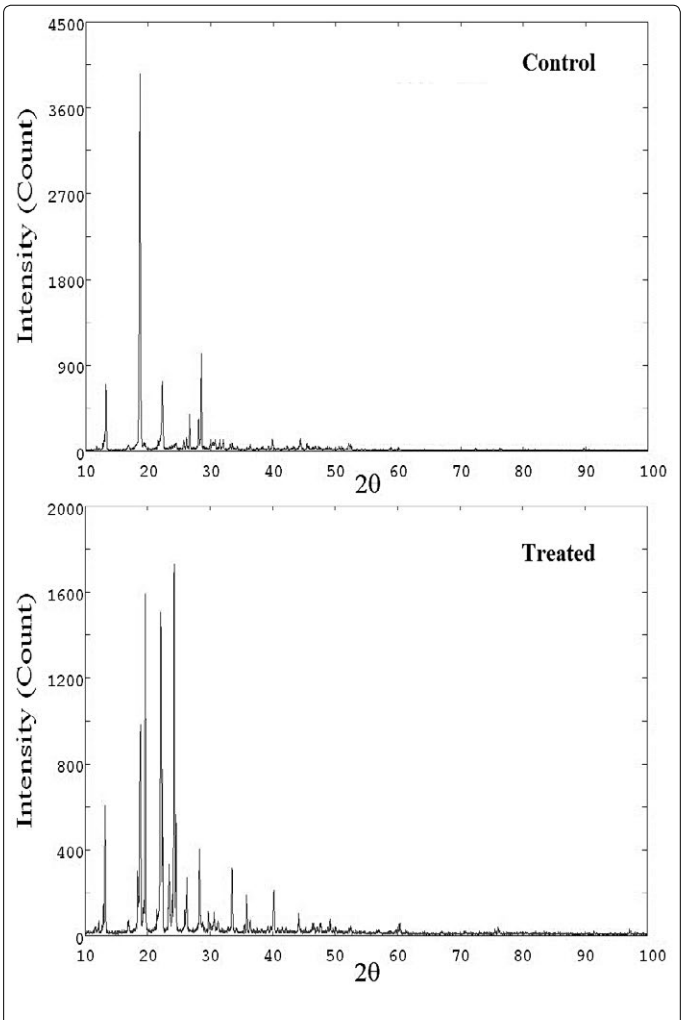

Figure 1: XRD diffractogram of *p*-anisidine.

TGA-DTG analysis

Thermogravimetric analysis is used to evaluate the vaporization, sublimation, and thermal degradation pattern of the samples. The TGA and DTG thermogram of control and treated samples of *p*-anisidine are shown in Figure 4 and the data are presented in Table 2. The onset temperature of thermal degradation was observed at 134.68°C and 150.02°C for the control and treated samples, respectively. While, the end-set temperature of thermal degradation was observed at 198.54°C and 206.21°C in the control and treated sample, respectively. This showed about 11.39% and 3.86% increase in the onset and end-set temperature, respectively after biofield treatment as compared to the control. Moreover, the percent weight loss during thermal decomposition was 70.07% in the control and 66.19% in the treated sample. The result showed decrease in percent weight loss during thermal decomposition after the biofield treatment. Based on this, it is presumed that biofield treated *p*-anisidine may be more thermally stable as compared to the control. The DTG thermogram exhibited the T_{max} (the temperature at which the sample lost its maximum weight) at 165.99°C in the control sample and at 168.10°C in the treated sample of *p*-anisidine. The result revealed about 1.27% increase in T_{max} of treated sample

Parameter	Control	Treated
Unit cell volume (10^{-23} cm^3)	683.81	690.18
Crystallite size (nm)	83.84	84.62
Molecular weight (g/mol)	124.79	125.95

Table 1: XRD data (volume of unit cell, crystallite size and molecular weight) of *p*-anisidine.

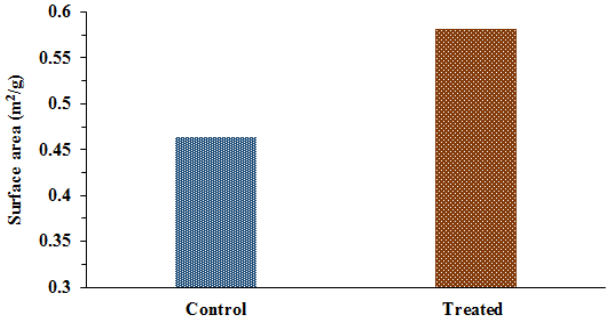

Figure 2: Surface area analysis of control and treated *p*-anisidine.

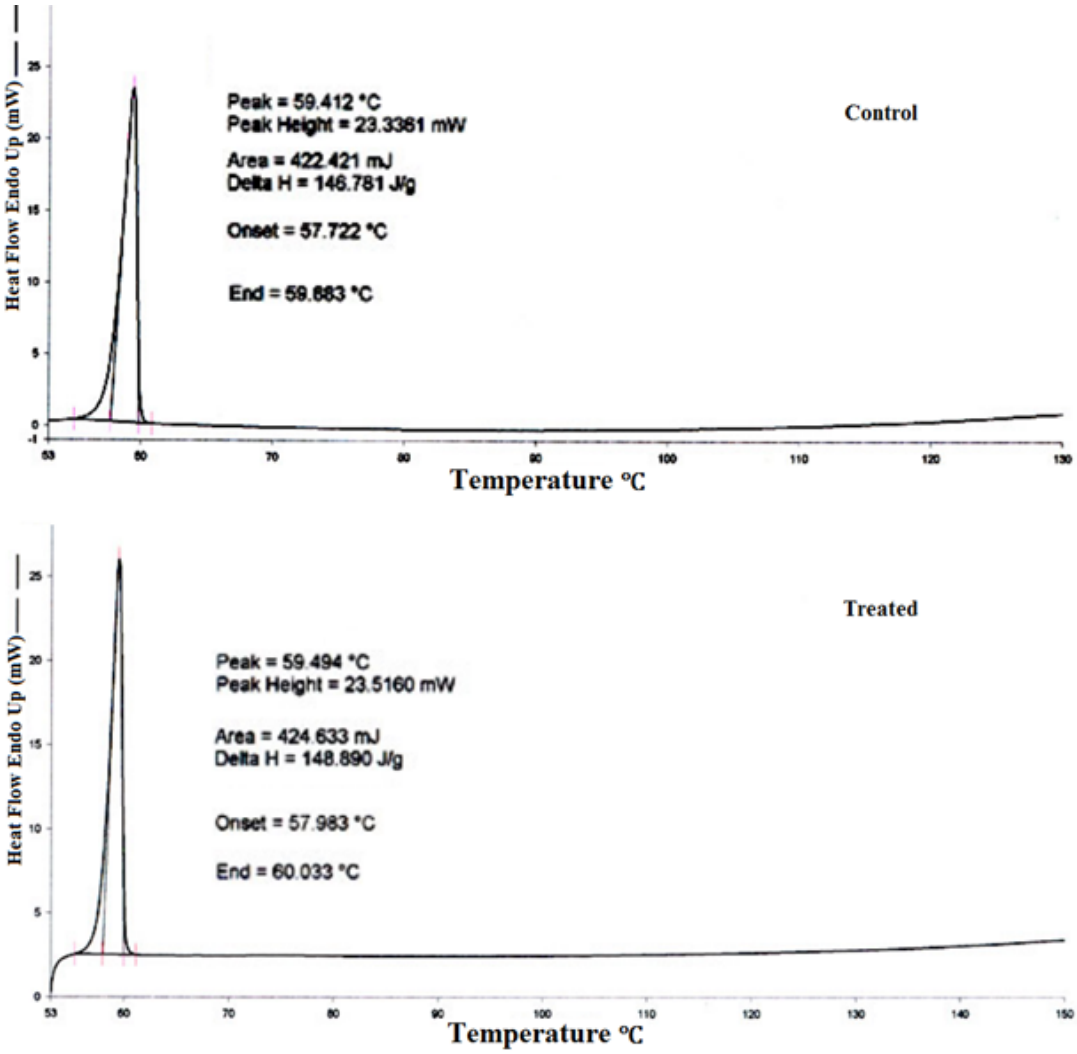

Figure 3: DSC thermogram of control and treated *p*-anisidine.

Parameter	Control	Treated
Latent heat of fusion (J/g)	146.78	148.89
Melting point (°C)	59.41	59.49
Onset temperature (°C)	134.68	150.02
End-set temperature (°C)	198.54	206.21
T_{max} (°C)	165.99	168.10

Table 2: Thermal analysis of control and treated samples of *p*-anisidine. T_{max}: Temperature at maximum weight loss occurs.

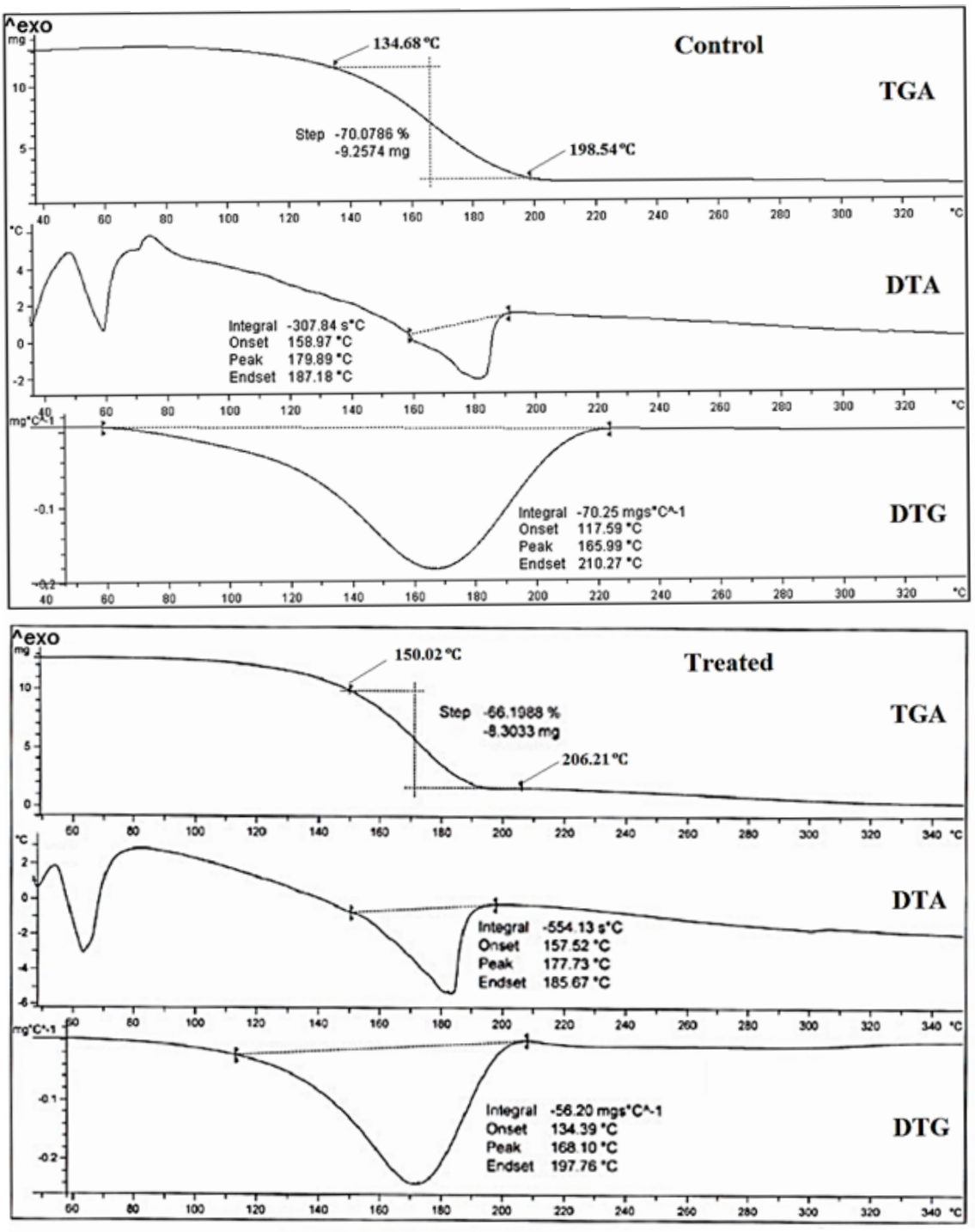

Figure 4: TGA-DTG thermogram of control and treated *p*-anisidine.

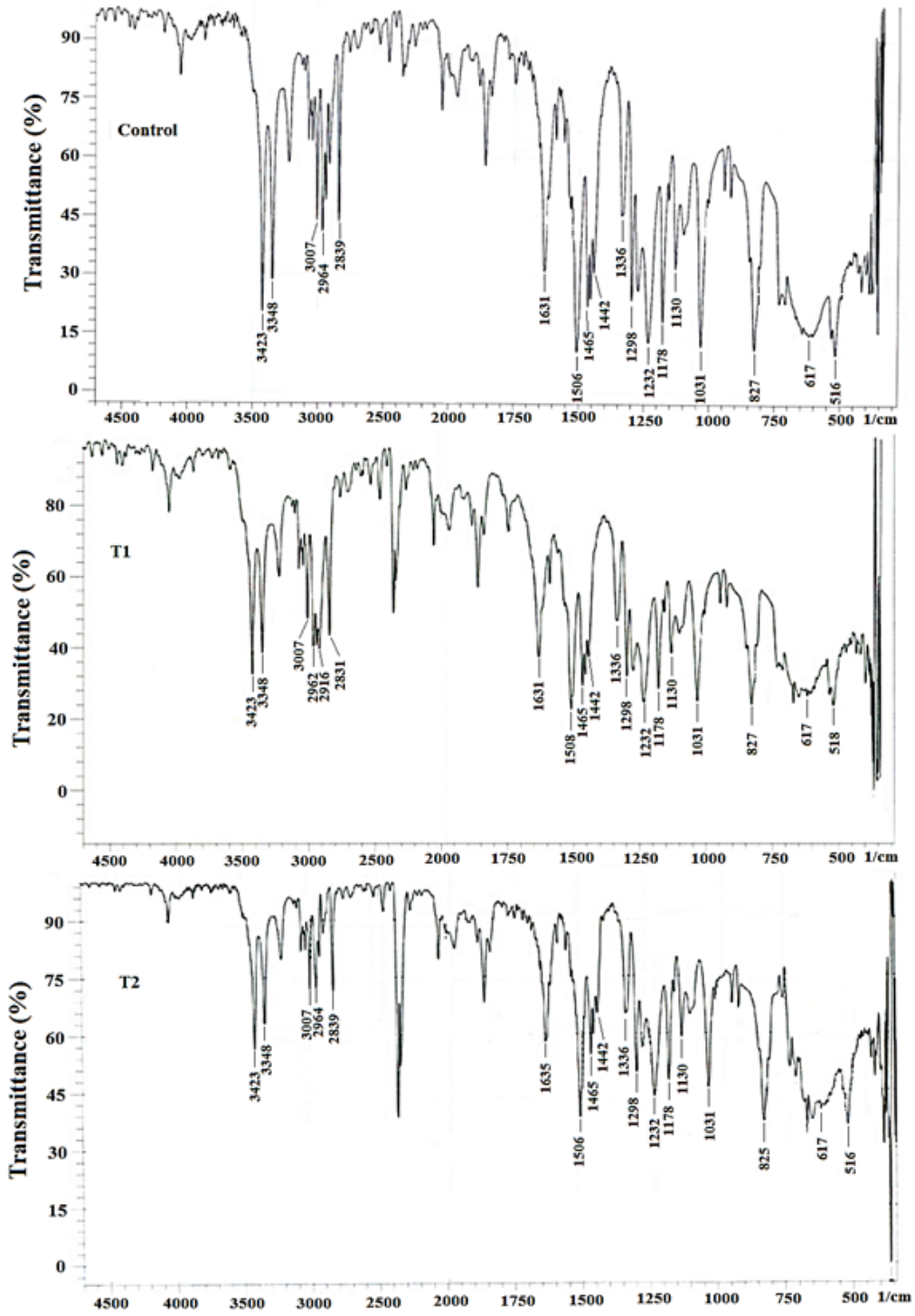

Figure 5: FT-IR spectra of control and treated (T1 and T2) *p*-anisidine.

with respect to the control. This increase in T_{max} in treated sample might be due to the alteration in internal energy through biofield energy treatment that results into enhanced thermal stability of treated sample as compared to the control. Overall, the result of this study showed the increase in onset temperature of thermal degradation and T_{max}. This might leads to decrease in the tendency of vaporization of p-anisidine molecule. As a result, the environmental contamination due to vapors of *p*-anisidine (which is the major cause of *p*-anisidine toxicity) should be decreased drastically.

FT-IR spectroscopic analysis

FT-IR spectra of the control and treated samples of *p*-anisidine (Figure 5) were inferred with the help of theoretically predicted wavenumber. The *p*-anisidine molecule contains N-H, =C-H, C=C,

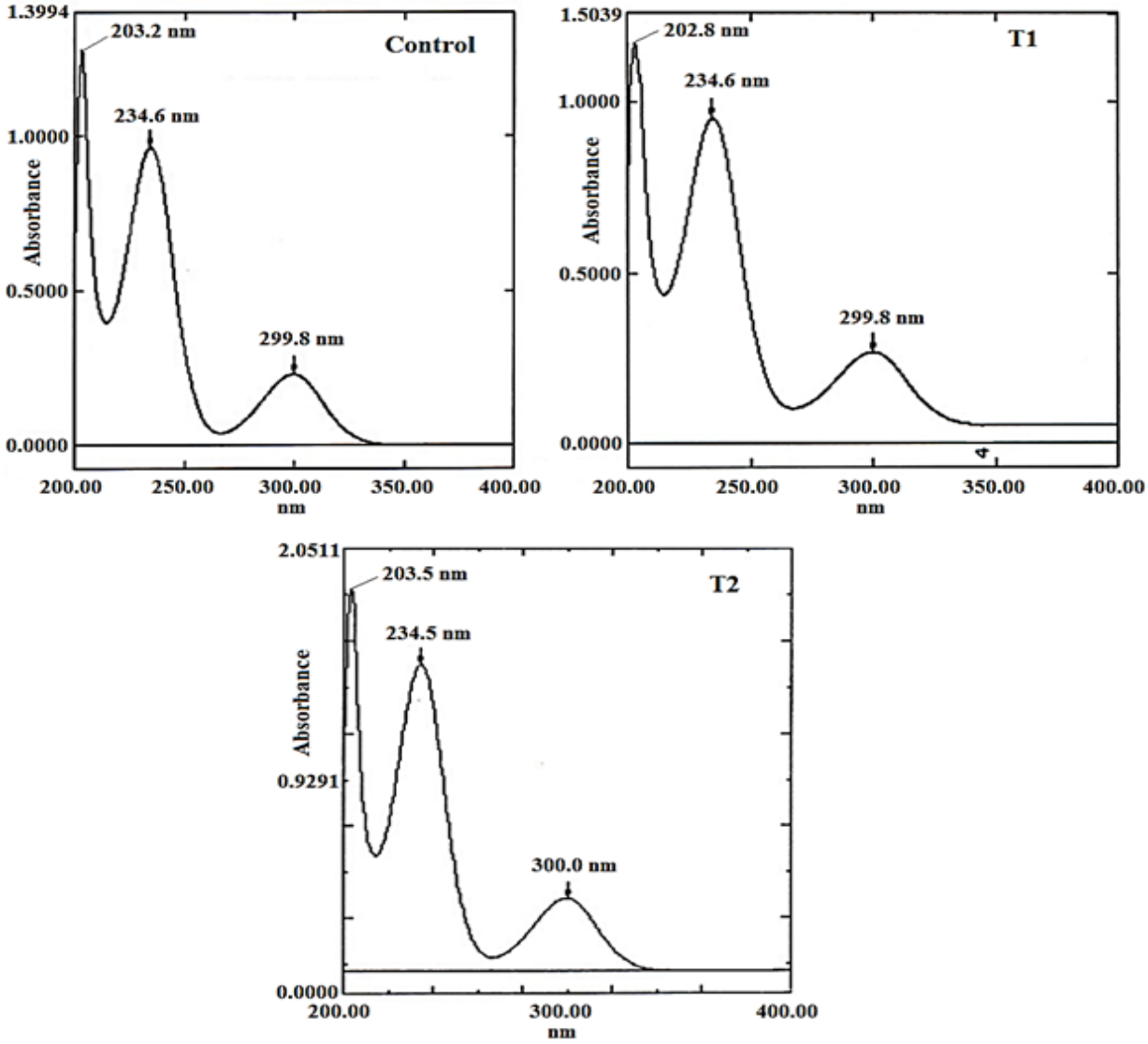

Figure 6: UV-Vis spectra of control and treated (T1 and T2) *p*-anisidine.

C-N, and C-O bond vibrations. The N-H stretching was assigned to peaks at 3348-3423 cm^{-1} in all the three samples i.e., the control and treated (T1 and T2). Likewise, the =C-H (aromatic) stretching was assigned to peak at 3007 cm^{-1} in all the three samples i.e., the control and treated (T1 and T2). The C-H stretching (methyl) was attributed to peaks appeared at 2839-2964 cm^{-1} in control, 2831-2962 cm^{-1} in T1 and 2839-2964 cm^{-1} in T2 sample. The aromatic C=C stretching of aromatic ring was appeared in the region of 1506-1631 cm^{-1} in control, 1508-1631 cm^{-1} in T1 and 1506-1635 cm^{-1} in T2 sample. The C-H asymmetrical and symmetrical bending peaks were observed in the region of 1442-1465 cm^{-1} in all the samples *i.e.,* control, T1 and T2. In addition, the C-N stretching peak was observed at 1336 cm^{-1} in all the three samples. The C-O stretching for ether linkage was observed at 1031, 1298 cm^{-1} in all the three samples. The =C-H in-plane deformation peaks were appeared at 1130-1178 cm^{-1} in all the three samples. Whereas, the C-H out of plane deformation peaks were appeared at 516-827 cm^{-1} control, 518-827 cm^{-1} in T1, and 516-825 cm^{-1} in T2 sample. The observed FT-IR spectra were well supported with the literature data [35].

UV-Vis spectroscopy

The UV spectra of both control and treated (T1 and T2) samples are presented in Figure 6. The UV spectrum of control *p*-anisidine showed the three different absorption maxima (λ_{max}) at 203.2, 234.6, and 299.8 nm. The UV spectrum of T1 sample showed the similar pattern of λ_{max} *i.e.,* at 202.8, 234.6, and 299.8 nm. Whereas, the T2 sample exhibited the λ_{max} at 203.5, 234.5, and 300.0 nm. The result suggested the similar pattern of λ_{max} in the treated samples as compared to the control. Overall, the UV-vis spectral analysis suggests that biofield energy treatment may not cause any significant change in the λ_{max} of treated *p*-anisidine samples with respect to the control.

Conclusions

In brief, the XRD diffractogram of biofield treated *p*-anisidine showed the slight increase in unit cell volume, crystallite size and molecular weight as compared to the control. The intensity of XRD peaks was also increased in treated sample as compared to the control. The surface area analysis showed a significant increase (25.44%) in the

surface area of biofield treated *p*-anisidine with respect to the control. The DSC analysis showed the slight increase in latent heat of fusion from 146.78 J/g (control) to 148.89 J/g in the treated sample. The TGA/DTG analysis showed the increase in onset and end set temperature of thermal degradation by 11.39% and 3.86%, respectively in treated sample with respect to the control. Moreover, the T_{max} was also increased slightly from 165.99 (control) to 168.10°C in treated sample of *p*-anisidine.

Overall, it can be concluded that Mr. Trivedi's biofield energy treatment has the impact on physical and thermal properties of *p*-anisidine with respect to the control. Based on this, it is assumed that biofield treated *p*-anisidine could be more useful as a chemical intermediate in the organic synthesis of various dyes and pharmaceuticals.

Acknowledgements

The authors like to acknowledge the Trivedi Science, Trivedi Master Wellness and Trivedi Testimonials for their steady support during the work. Authors would also like to thanks the whole team from the MGV pharmacy college, Nasik for providing the instrumental facility.

References

1. Del Valle MA, Gacitua MA, Borrego ED, Zamora PP, Diaz FR, et al. (2012) Electro-synthesis and characterization of aniline and *o*-anisidine oligomers. Int J Electrochem Sci 7: 2552-2565.
2. Elsersawi A (2009) Chemistry, biology and cancer: The bond. Xlibris Corporation, USA.
3. Harbison RD, Bourgeois MM, Johnson GT (2015) Hamilton and Hardy's industrial toxicology. 6th edn. John Wiley & Sons, New Jersey, USA.
4. WHO (1982) IARC Monographs on the evaluation of the carcinogenic risk of chemicals to humans. Some aromatic amines, anthraquinones and nitroso compounds, and inorganic fluorides use in drinking-water and dental preparations. Cancer 27.
5. Singh BP, Nyska A, Kissling GE, Lieuallen W, Johansson SL, et al. (2010) Urethral carcinoma and hyperplasia in male and female $B_6C_3F_1$ mice treated with 3,3',4,4'-tetrachloroazobenzene (TCAB). Toxicol Pathol 38: 372-381.
6. Hok J, Tishelman C, Ploner A, Forss A, Falkenberg T (2008) Mapping patterns of complementary and alternative medicine use in cancer: An explorative cross-sectional study of individuals with reported positive "exceptional" experiences. BMC Complement Altern Med 8: 48.
7. Koithan M (2009) Introducing complementary and alternative therapies. J Nurse Pract 5: 18-20.
8. Aldridge D (1991) Spirituality, healing and medicine. Br J Gen Pract 41: 425-427.
9. Cahil M (1998) Nurses handbook of complementary and alternative therapies. Springhouse, PA: Springhouse Corporation.
10. Movaffaghi Z, Farsi M (2009) Biofield therapies: Biophysical basis and biological regulations? Complement Ther Clin Pract 15: 35-37.
11. Maxwell JC (1865) A dynamical theory of the electromagnetic field. Phil Trans R Soc Lond 155: 459-512.
12. Rubik B (2002) The biofield hypothesis: Its biophysical basis and role in medicine. J Altern Complement Med 8: 703-717.
13. Rubik B, Brooks AJ, Schwartz GE (2006) *In vitro* effect of Reiki treatment on bacterial cultures: Role of experimental context and practitioner wellbeing. J Altern Complement Med 12: 7-13.
14. Benor DJ (1990) Survey of spiritual healing research. Complement Med Res 4: 9-33.
15. Rein G (1995) The *in vitro* effect of bioenergy on conformational state of human DNA in aqueous solutions. Acupunct Electrother Res 20: 173-180.
16. Trivedi MK, Tallapragada RM, Branton A, Trivedi D, Nayak G, et al. (2015) Potential impact of biofield treatment on atomic and physical characteristics of magnesium. Vitam Miner 3: 129.
17. Trivedi MK, Patil S, Tallapragada RM (2013) Effect of biofield treatment on the physical and thermal characteristics of silicon, tin and lead powders. J Material Sci Eng 2: 125.
18. Trivedi MK, Nayak G, Patil S, Tallapragada RM, Latiyal O (2015) Evaluation of biofield treatment on physical, atomic and structural characteristics of manganese (II, III) oxide. J Material Sci Eng 4: 177.
19. Trivedi MK, Patil S, Shettigar H, Bairwa K, Jana S (2015) Spectroscopic characterization of chloramphenicol and tetracycline: An impact of biofield. Pharm Anal Acta 6: 395.
20. Trivedi MK, Patil S, Shettigar H, Bairwa K, Jana S (2015) Spectroscopic characterization of biofield treated metronidazole and tinidazole. Med Chem 5: 340-344.
21. Nayak G, Altekar N (2015) Effect of biofield treatment on plant growth and adaptation. J Environ Health Sci 1: 1-9.
22. Lenssen AW (2013) Biofield and fungicide seed treatment influences on soybean productivity, seed quality and weed community. Agricultural Journal 8: 138-143.
23. Shinde V, Sances F, Patil S, Spence A (2012) Impact of biofield treatment on growth and yield of lettuce and tomato. Aust J Basic Appl Sci 6: 100-105.
24. Trivedi MK, Patil S, Shettigar H, Mondal SC, Jana S (2015) Evaluation of biofield modality on viral load of Hepatitis B and C viruses. J Antivir Antiretrovir 7: 83-88.
25. Trivedi MK, Patil S, Shettigar H, Gangwar M, Jana S (2015) Antimicrobial sensitivity pattern of *Pseudomonas fluorescens* after biofield treatment. J Infect Dis Ther 3: 222.
26. Patterson AL (1939) The Scherrer formula for X-Ray particle size determination. Phys Rev 56: 978-982.
27. Pavia DL, Lampman GM, Kriz GS (2001) Introduction to spectroscopy. (3rdedn), Thomson Learning, Singapore.
28. Inoue M, Hirasawa I (2013) The relationship between crystal morphology and XRD peak intensity on $CaSO_4.2H_2O$. J Cryst Growth 380: 169-175.
29. Fultz B, Howe JM (2002) In Transmission electron microscopy and diffractometry of materials. Diffraction and the X-ray powder diffractometer. 4th edn. Springer-Verlag: Berlin.
30. Gaber A, Abdel-Rahim MA, Abdel-Latief AY, Abdel-Salam MN (2014) Influence of calcination temperature on the structure and porosity of nanocrystalline SnO_2 synthesized by a conventional precipitation method. Int J Electrochem Sci 9: 81-95.
31. Raj KJA, Viswanathan B (2009) Effect of surface area, pore volume, particle size of P25 titania on the phase transformation of anatase to rutile. Indian J Chem 48A: 1378-1382.
32. Groza JR, Shackelford JF (2007) Materials processing handbook. Taylor and Francis group, CRC Press.
33. Trivedi MK, Nayak G, Patil S, Tallapragada RM, Latiyal O (2015) Studies of the atomic and crystalline characteristics of ceramic oxide nano powders after bio field treatment. Ind Eng Manage 4: 161.
34. http://www.merckmillipore.com/IN/en/product/*p*-Anisidine,MDA_CHEM-845003.
35. http://www.chem.ucla.edu/~bacher/General/30BL/problems/spectroscopy/assignmentW14/key.html.